Electronic Supplementary Information

New carvacrol and thymol derivatives as potential insecticides: synthesis, biological activity, computational studies and nanoencapsulation

Carolina M. Natal[a], Maria José G. Fernandes[a], Nuno F. S. Pinto[a], Renato B. Pereira[b], Tatiana F. Vieira[c], Ana Rita O. Rodrigues[d], David M. Pereira[b], Sérgio F. Sousa[c], A. Gil Fortes[a], Elisabete M. S. Castanheira[d], M. Sameiro T. Gonçalves*[a]

[a.] *Centre of Chemistry, Department of Chemistry, University of Minho, Campus of Gualtar, 4710-057 Braga, Portugal. E-mail:msameiro@quimica.uminho.pt*

[b.] *REQUIMTE/LAQV, Laboratory of Pharmacognosy, Department of Chemistry, Faculty of Pharmacy, University of Porto, R. Jorge Viterbo Ferreira, 228, 4050-313 Porto, Portugal*

[c.] *Associate Laboratory i4HB - Institute for Health and Bioeconomy, Faculty of Medicine, University of Porto, 4200-319 Porto, Portugal*

[d.] *UCIBIO – Applied Molecular Biosciences Unit, BioSIM - Department of Biomedicine, Faculty of Medicine, University of Porto, 4200-319 Porto, Portugal*

[e.] *Centre of Physics of Minho and Porto Universities (CF-UM-UP), University of Minho, Campus of Gualtar, 4710-057 Braga, Portugal*

1. ^{1}H and ^{13}C NMR spectra of compounds 3a-c, 4a-c, 5, 6 and 8

^{1}H NMR spectra of compounds **3a**-**c**, **4a**-**c**, **5**, **6** and **8** are shown. These spectra confirm the corresponding structure and purity of each compound. In addition, ^{13}C spectra are also shown. This information serves as the statement for confirming the purity (≥95%) of the compounds extracted**/**synthesized in the reported work.

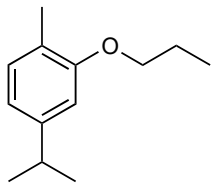

3a

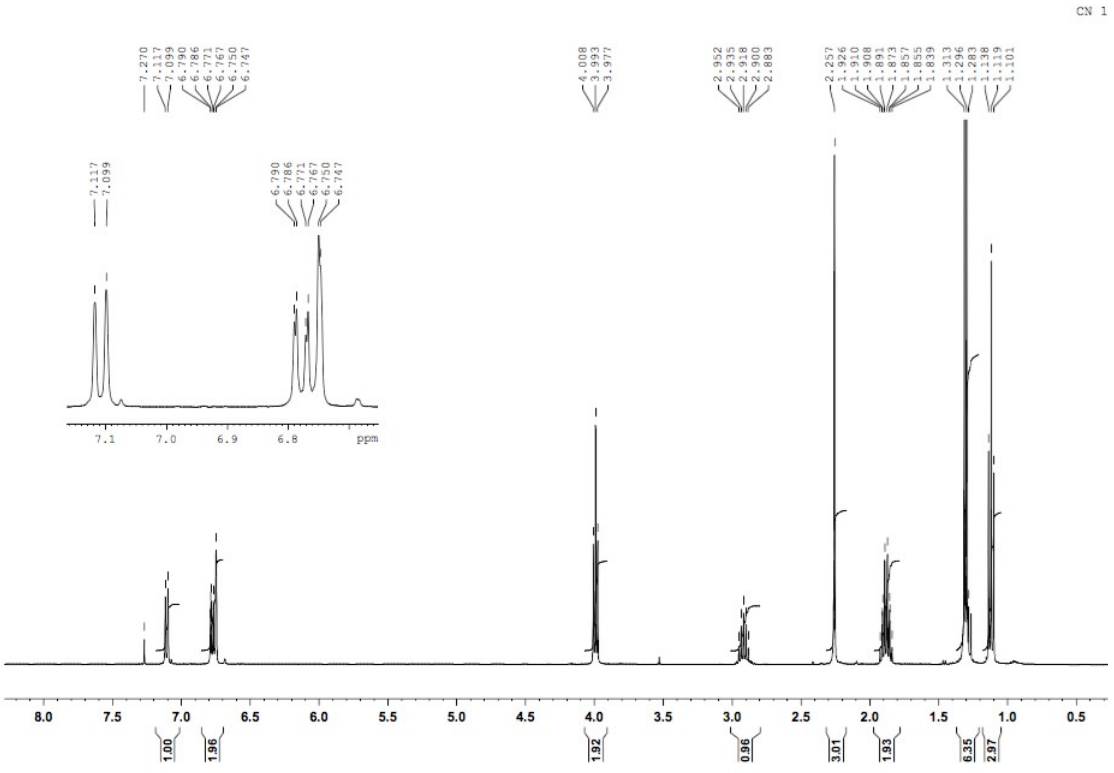
CN 1
7.270
7.117
7.099
6.790
6.786
6.771
6.767
6.750
6.747
4.008
3.993
3.977
2.952
2.935
2.918
2.900
2.883
2.257
1.926
1.910
1.908
1.891
1.873
1.857
1.855
1.839
1.333
1.286
1.283
1.138
1.119
1.101
7.1
7.0
6.9
6.8
ppm
8.0
7.5
7.0
6.5
6.0
5.5
5.0
4.5
4.0
3.5
3.0
2.5
2.0
1.5
1.0
0.5
1.00
1.96
1.92
0.96
3.01
1.93
6.35
2.97

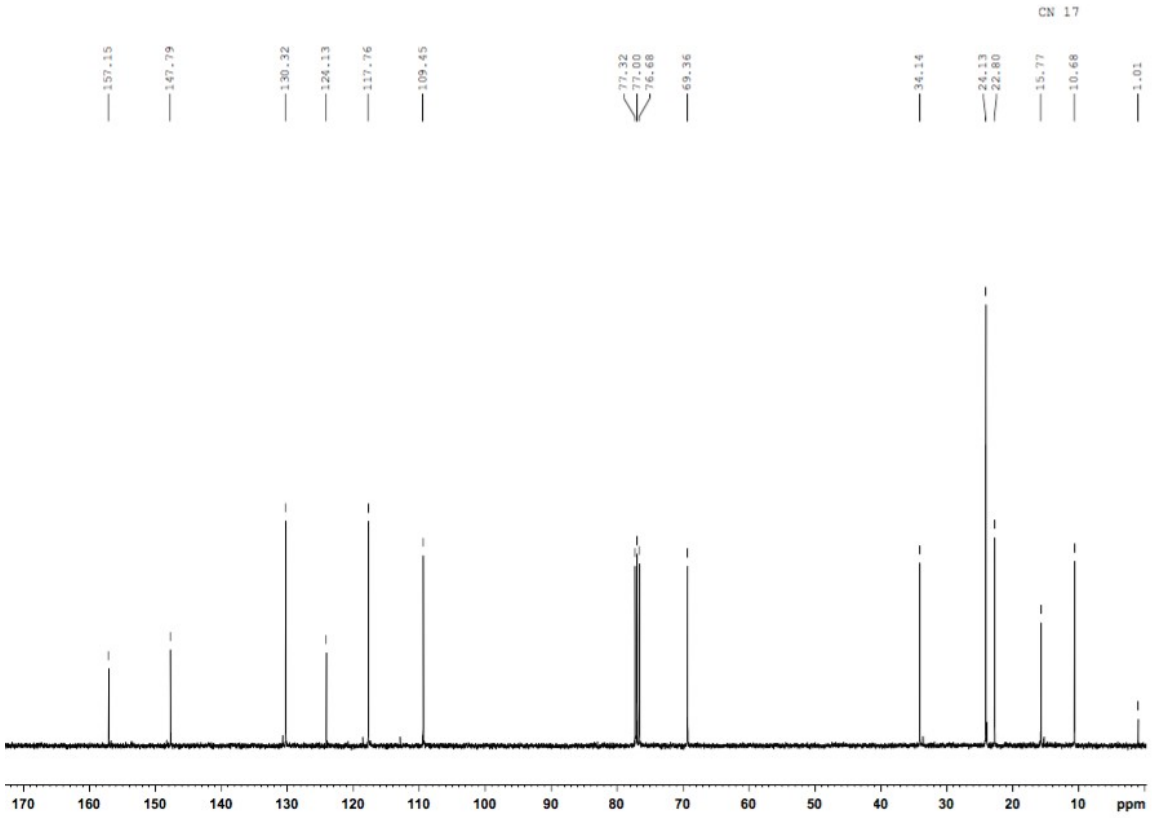
CN 17
157.15
147.79
130.32
124.13
117.76
109.45
77.32
77.00
76.68
69.36
34.14
24.13
22.80
15.77
10.68
1.01
170
160
150
140
130
120
110
100
90
80
70
60
50
40
30
20
10
ppm

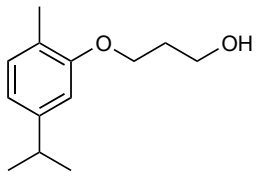
O
OH

3b

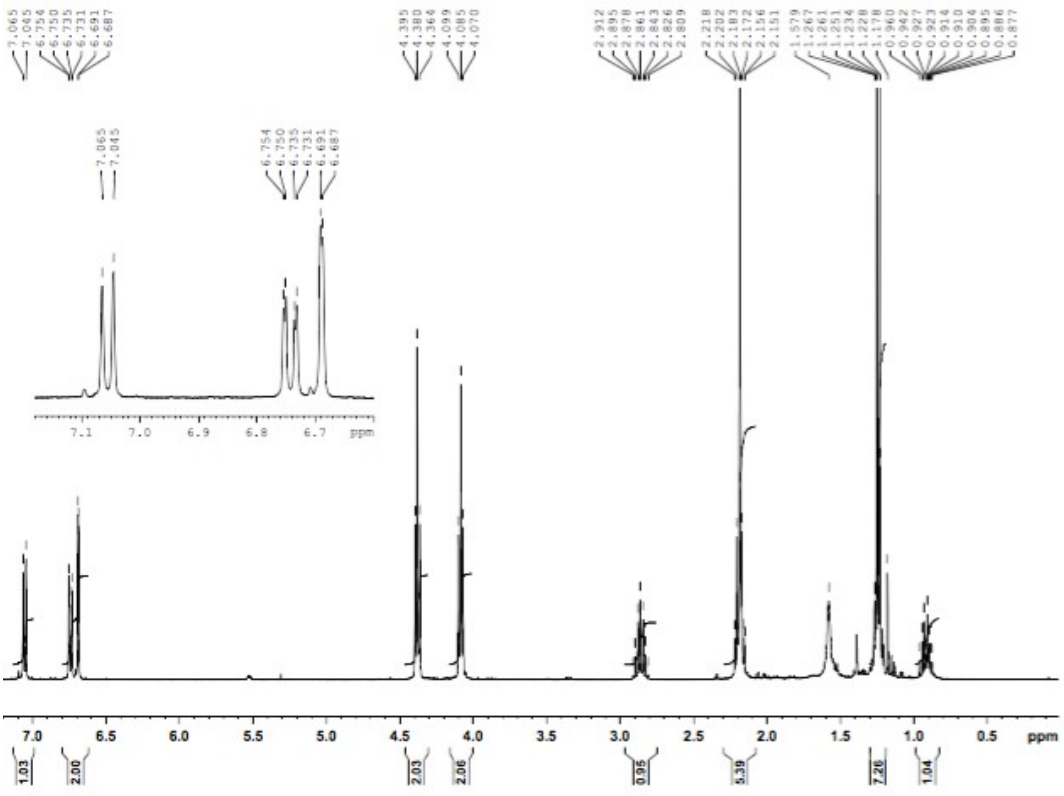
7.065
7.045
6.754
6.750
6.735
6.731
6.691
6.687
4.395
4.380
4.366
4.099
4.085
4.070
2.912
2.895
2.878
2.861
2.843
2.826
2.809
2.218
2.202
2.183
2.172
2.156
2.151
1.579
1.267
1.261
1.251
1.234
1.220
1.178
0.960
0.942
0.927
0.923
0.914
0.910
0.904
0.895
0.886
0.877
7.1
7.0
6.9
6.8
6.7
ppm
7.0
6.5
6.0
5.5
5.0
4.5
4.0
3.5
3.0
2.5
2.0
1.5
1.0
0.5
ppm
1.03
2.00
2.03
2.06
0.95
5.39
7.26
1.04

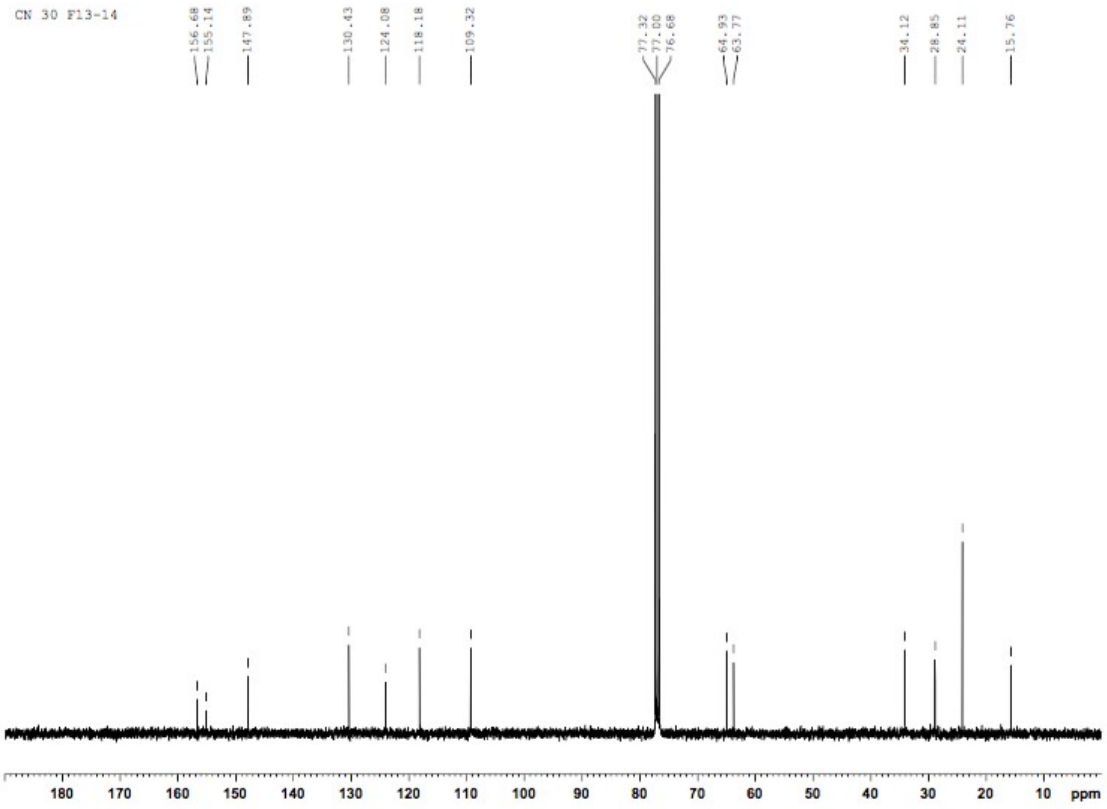
CN 30 F13-14
156.68
155.14
147.89
130.43
124.08
118.18
109.32
77.32
77.00
76.68
64.93
63.77
34.12
28.85
24.11
15.76
180
170
160
150
140
130
120
110
100
90
80
70
60
50
40
30
20
10
ppm

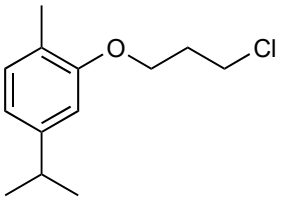
O
Cl

3c

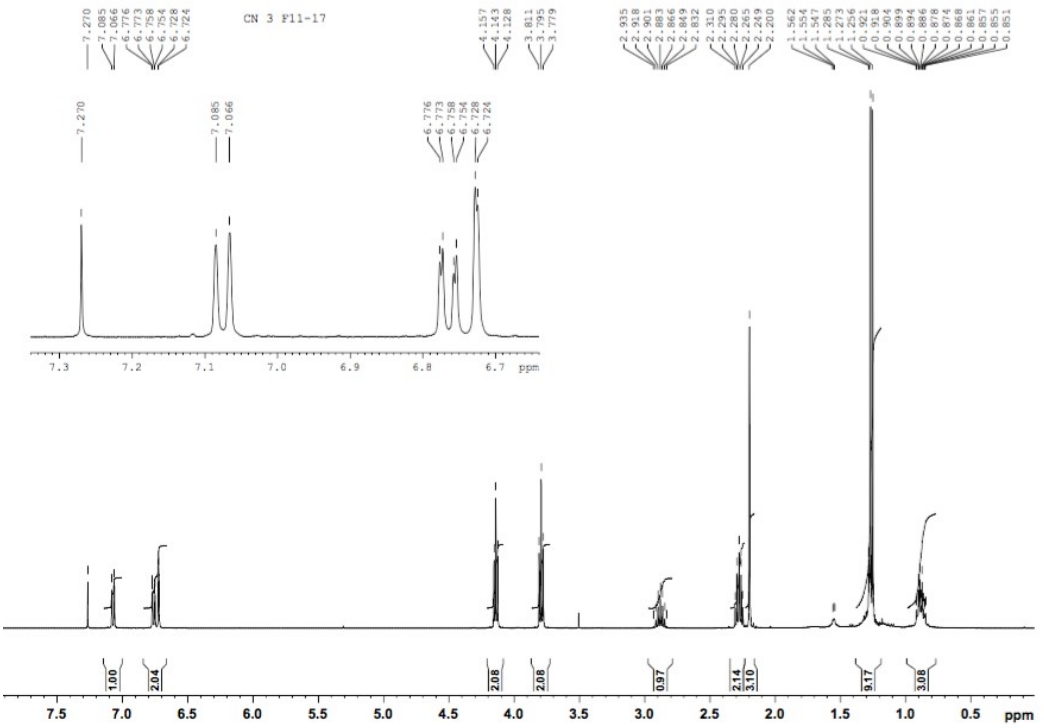
CN 3 F11-17
7.270
7.085
7.066
6.776
6.773
6.758
6.754
6.728
6.724
4.157
4.143
4.128
3.811
3.795
3.779
2.935
2.918
2.901
2.883
2.866
2.849
2.832
2.310
2.295
2.280
2.265
2.249
2.200
1.562
1.554
1.547
1.285
1.273
1.256
0.921
0.918
0.904
0.899
0.894
0.886
0.878
0.874
0.868
0.861
0.857
0.855
0.851
7.3
7.2
7.1
7.0
6.9
6.8
6.7
ppm
1.00
2.04
2.08
2.08
0.97
2.14
3.10
9.17
3.08
7.5
7.0
6.5
6.0
5.5
5.0
4.5
4.0
3.5
3.0
2.5
2.0
1.5
1.0
0.5
ppm

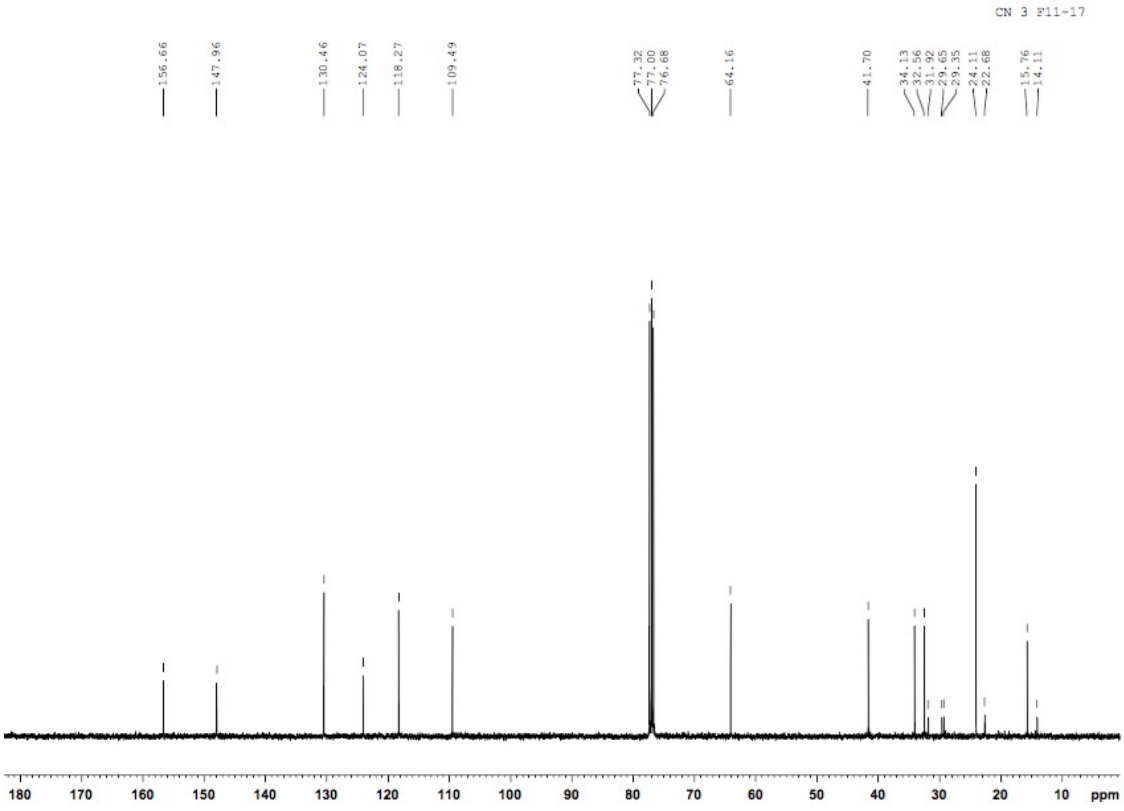
CN 3 F11-17
156.66
147.96
130.46
124.07
118.27
109.49
77.32
77.00
76.68
64.16
41.70
34.13
32.56
31.92
29.65
29.35
24.11
22.68
15.76
14.11
180
170
160
150
140
130
120
110
100
90
80
70
60
50
40
30
20
10
ppm

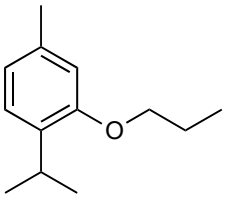

4a

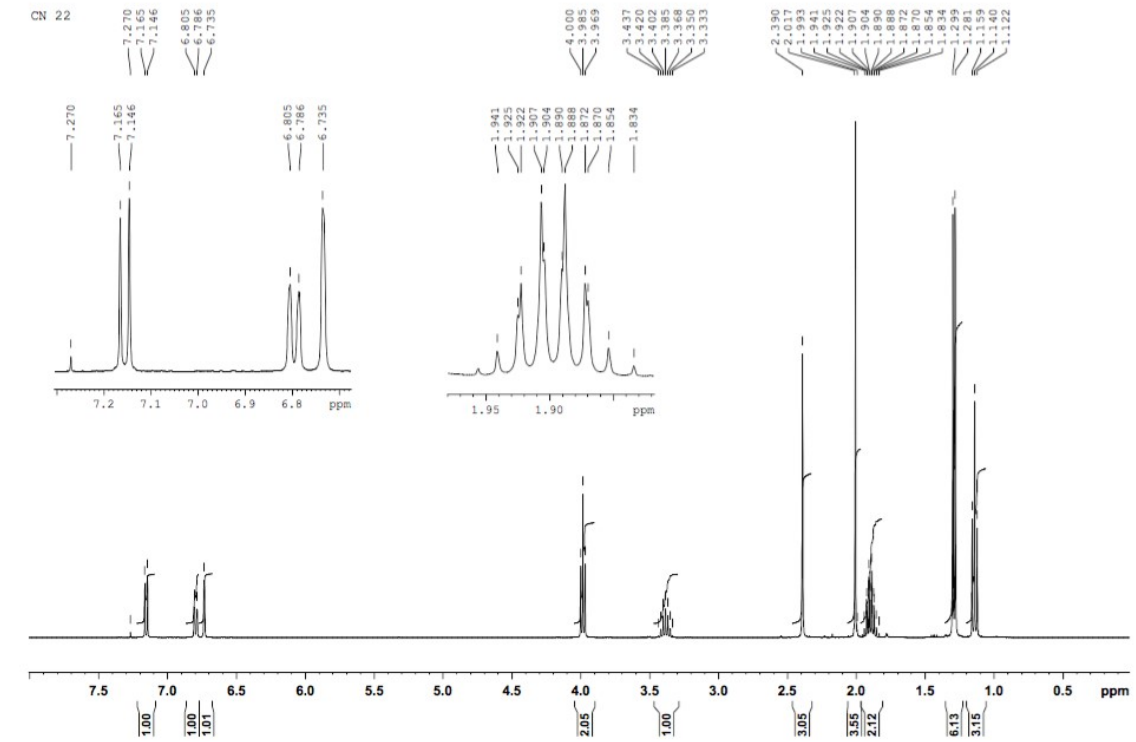
CN 22
7.270
7.165
7.146
6.805
6.786
6.735
4.000
3.985
3.969
3.437
3.420
3.402
3.385
3.368
3.350
3.333
2.390
2.017
1.993
1.941
1.925
1.922
1.907
1.904
1.890
1.888
1.872
1.870
1.854
1.834
1.299
1.281
1.259
1.140
1.122
ppm
1.00
1.00
1.01
2.05
1.00
3.05
3.55
2.12
6.13
3.15

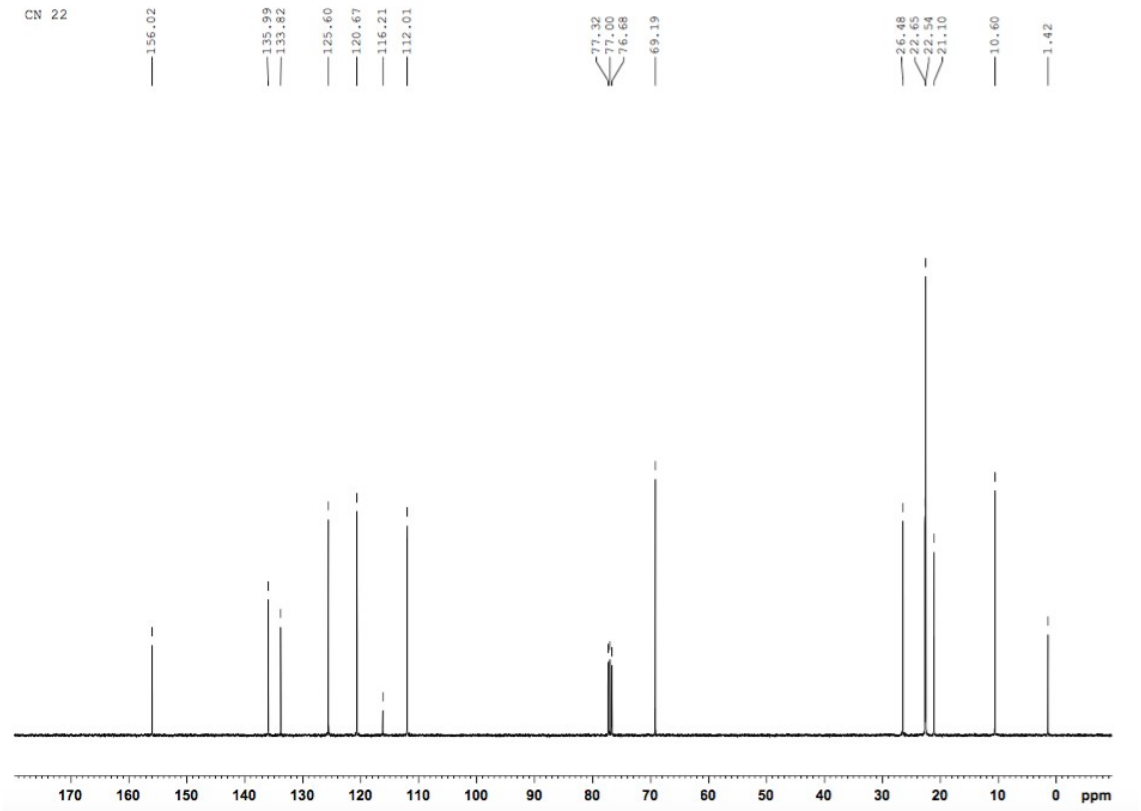
CN 22
156.02
135.99
133.82
125.60
120.67
116.21
112.01
77.32
77.00
76.68
69.19
26.48
22.65
22.54
21.10
10.60
1.42
ppm

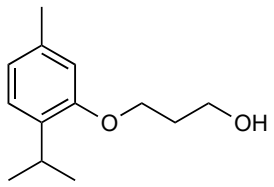
O
OH

4b

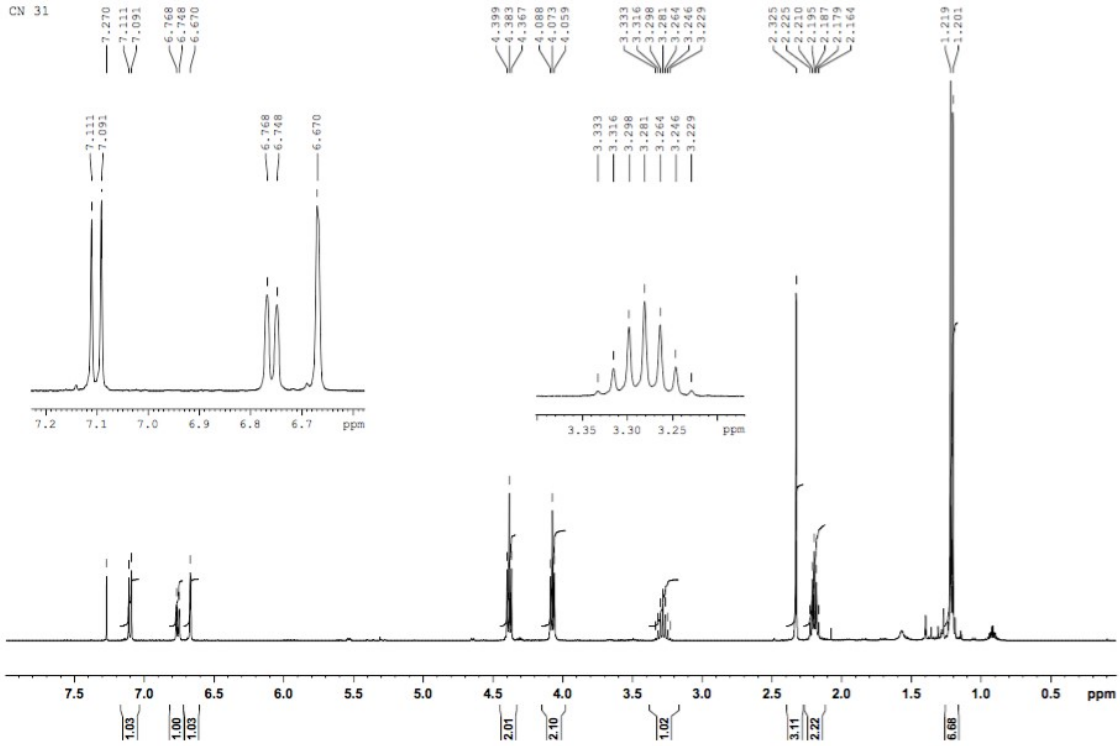
CN 31
7.270
7.111
7.091
6.768
6.748
6.670
4.399
4.383
4.367
4.088
4.073
4.059
3.333
3.316
3.298
3.281
3.264
3.246
3.229
2.325
2.225
2.210
2.195
2.187
2.179
2.164
1.219
1.201
ppm
1.03
1.00
1.03
2.01
2.10
1.02
3.11
2.22
6.68

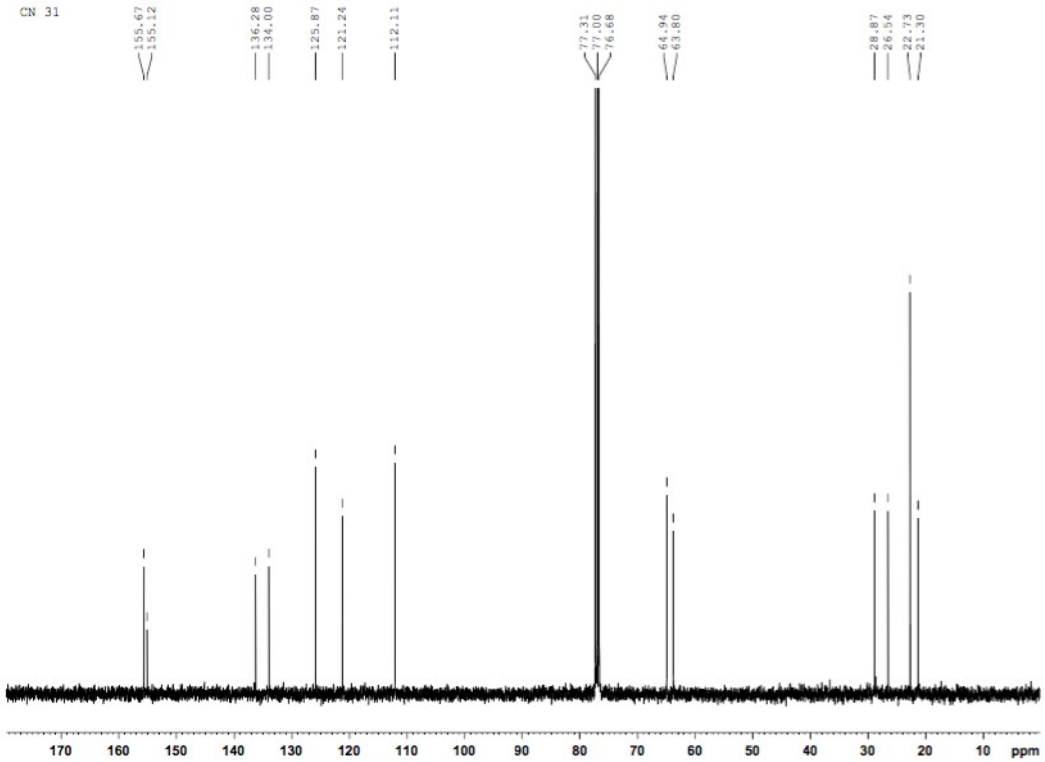
CN 31
155.67
155.12
136.28
134.00
125.87
121.24
112.11
77.31
77.00
76.68
64.94
63.80
28.87
26.54
22.73
21.30
ppm

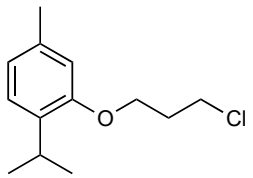
O
Cl

4c

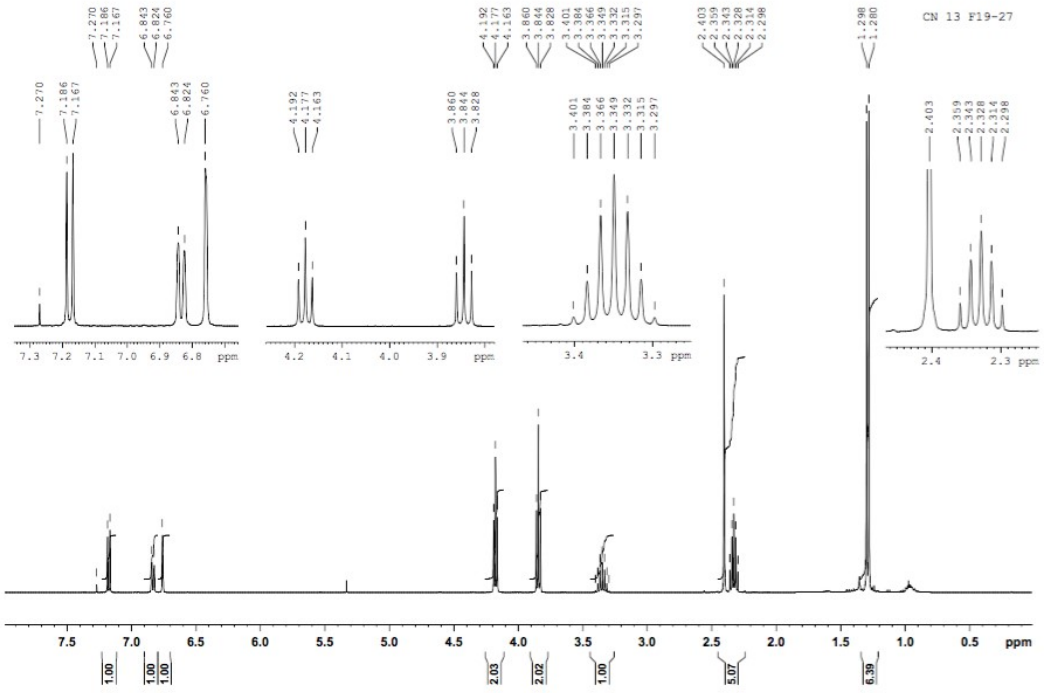
CN 13 F19-27
7.270
7.186
7.167
6.843
6.824
6.760
4.192
4.177
4.163
3.860
3.844
3.828
3.401
3.384
3.366
3.349
3.332
3.315
3.297
2.403
2.359
2.343
2.328
2.314
2.298
1.298
1.280
ppm

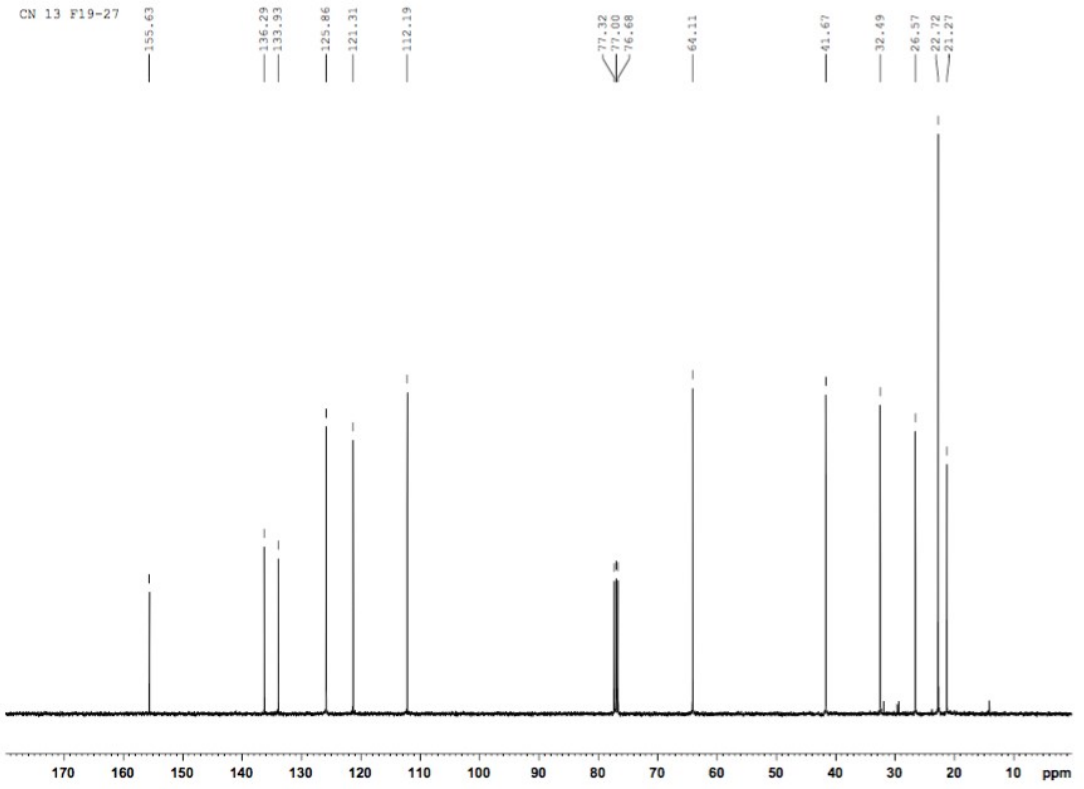
CN 13 F19-27
155.63
136.29
133.93
125.86
121.31
112.19
77.32
77.00
76.68
64.11
41.67
32.49
26.57
22.72
21.27
ppm

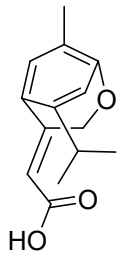
O
O
HO

6

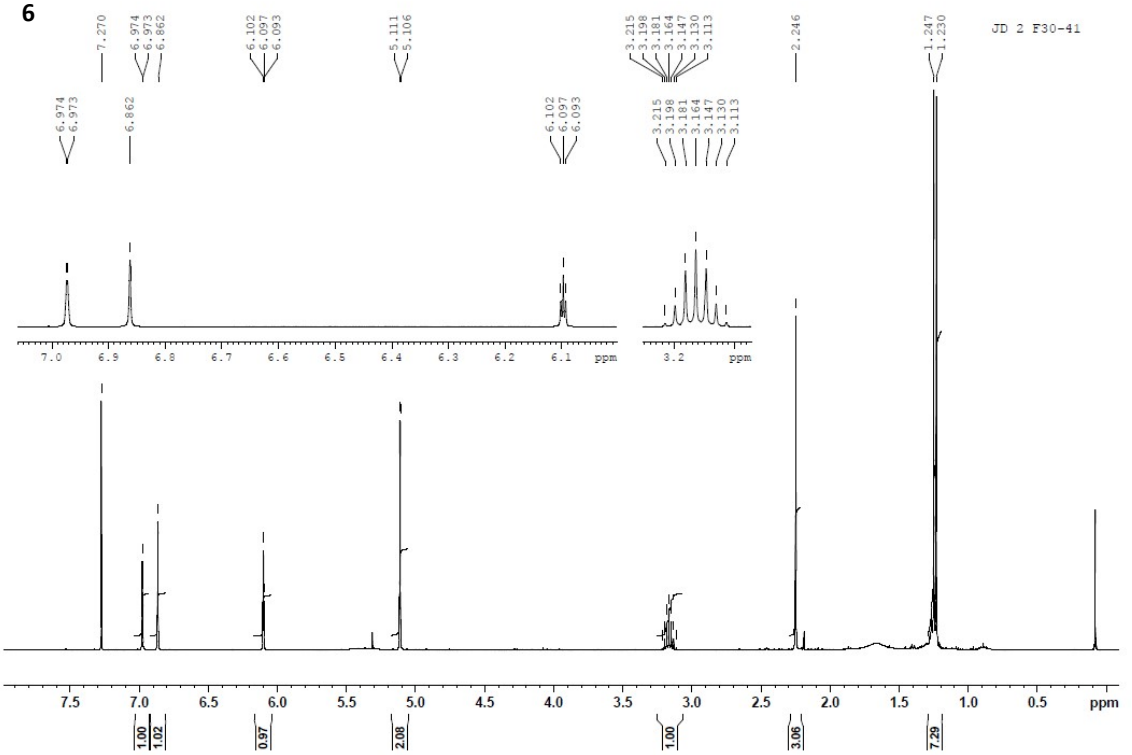
JD 2 F30-41
7.270
6.974
6.973
6.862
6.102
6.097
6.093
5.111
5.106
3.215
3.198
3.181
3.164
3.147
3.130
3.113
2.246
1.247
1.230
ppm
1.00
1.02
0.97
2.08
1.00
3.06
7.29

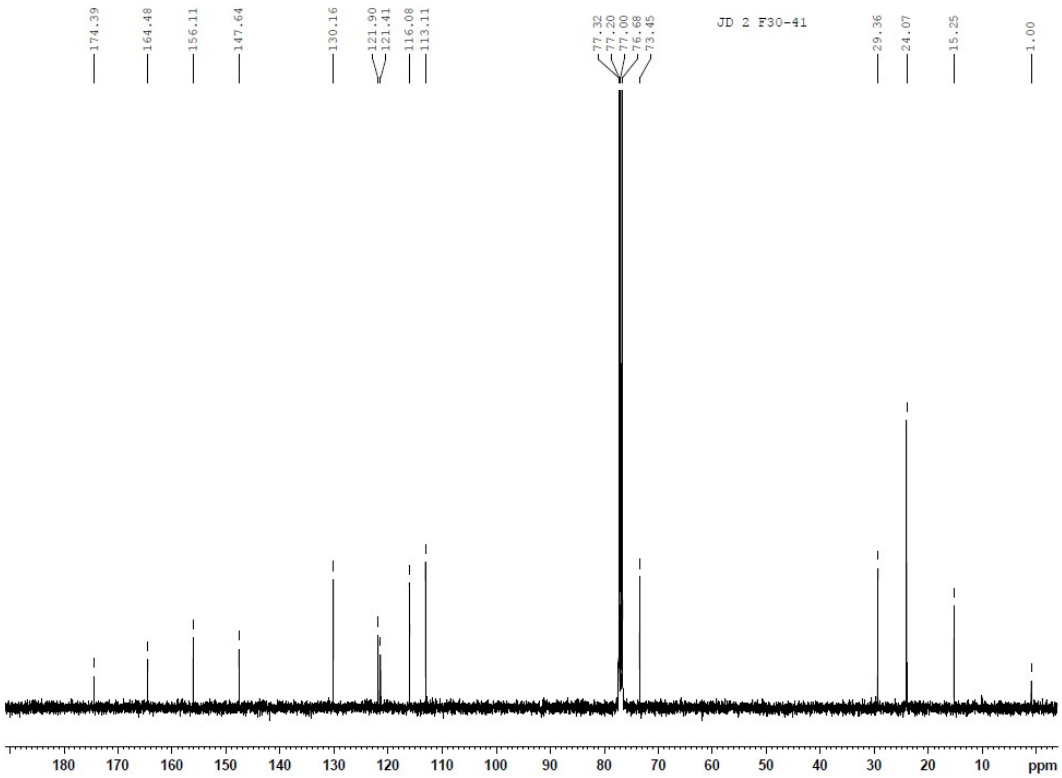
JD 2 F30-41
174.39
164.48
156.11
147.64
130.16
121.90
121.41
116.08
113.11
77.32
77.20
77.00
76.68
73.45
29.36
24.07
15.25
1.00
ppm

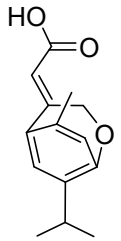
HO
O
O

6

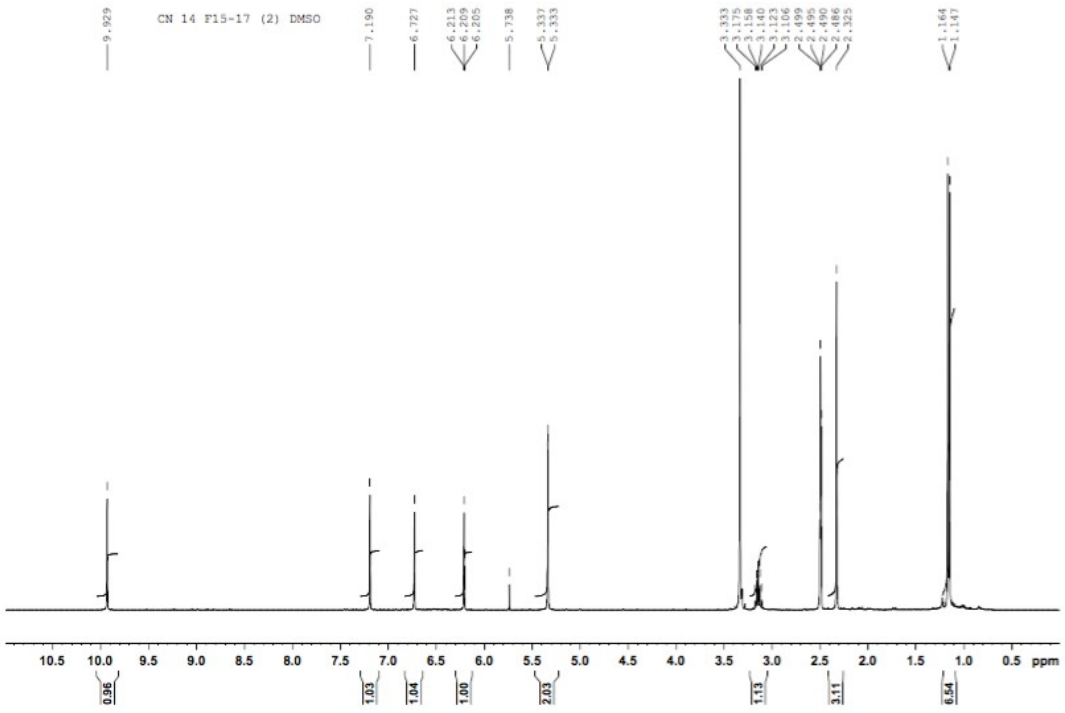
CN 14 F15-17 (2) DMSO
9.929
7.190
6.727
6.213
6.209
6.205
5.738
5.337
5.333
3.333
3.175
3.158
3.140
3.123
3.106
2.499
2.496
2.490
2.486
2.325
1.164
1.147
10.5 10.0 9.5 9.0 8.5 8.0 7.5 7.0 6.5 6.0 5.5 5.0 4.5 4.0 3.5 3.0 2.5 2.0 1.5 1.0 0.5 ppm
0.96
1.03
1.04
1.00
2.03
1.13
3.11
6.54

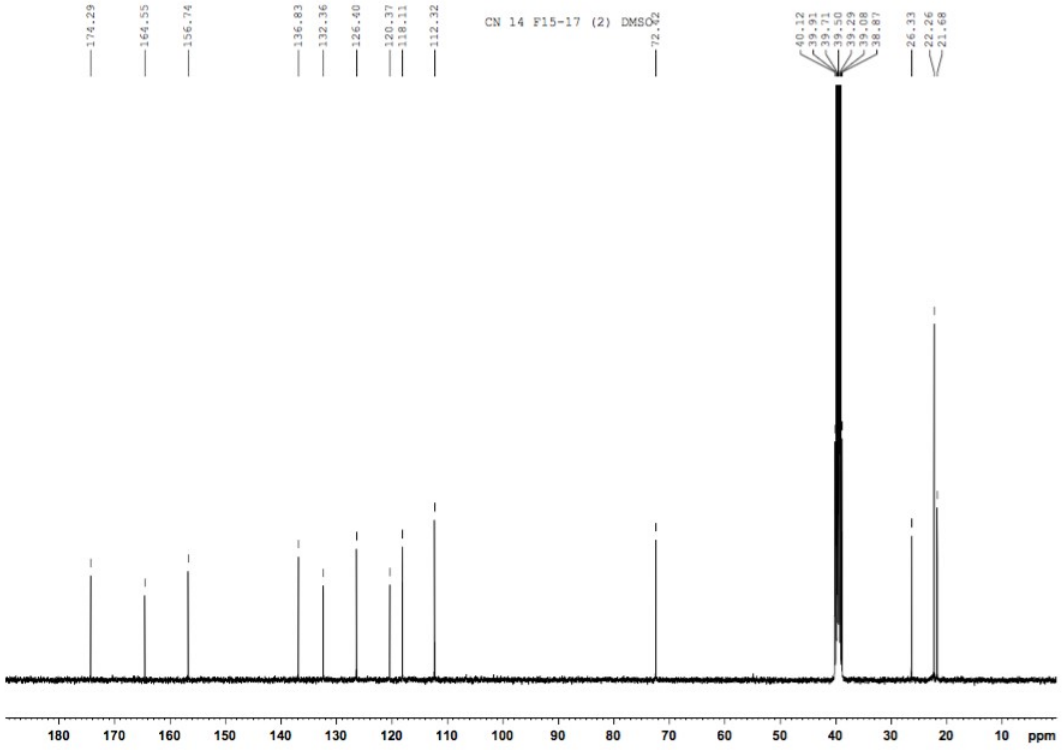
174.29
164.55
156.74
136.83
132.36
126.40
120.37
118.11
112.32
CN 14 F15-17 (2) DMSO
72.42
40.12
39.91
39.71
39.50
39.29
39.08
38.87
26.33
22.26
21.68
180 170 160 150 140 130 120 110 100 90 80 70 60 50 40 30 20 10 ppm

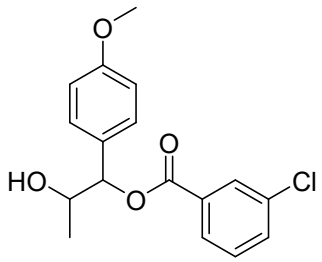

8

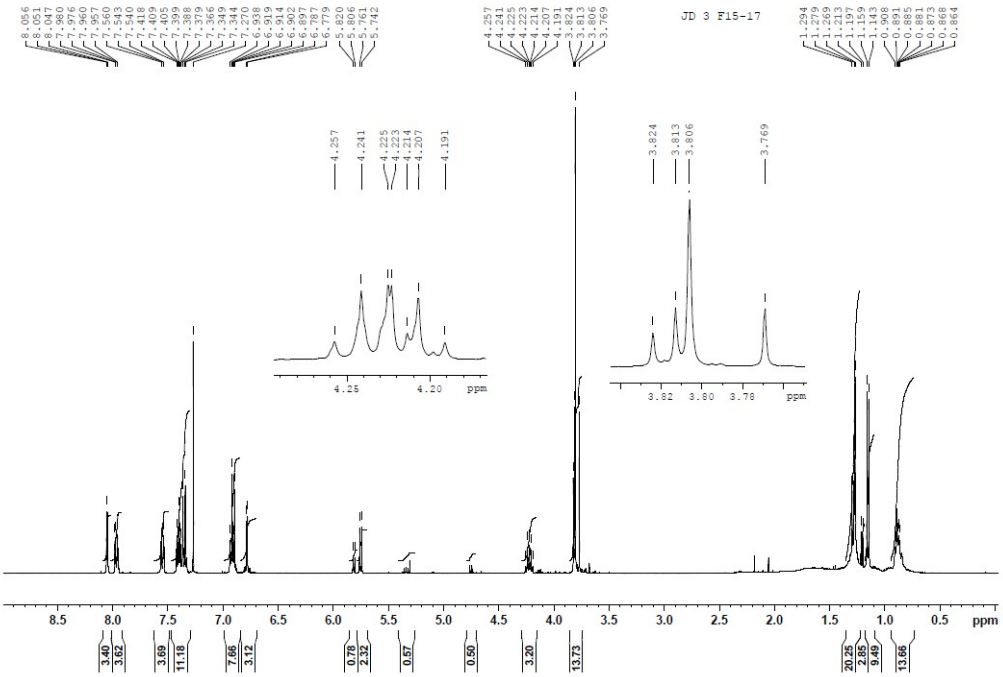

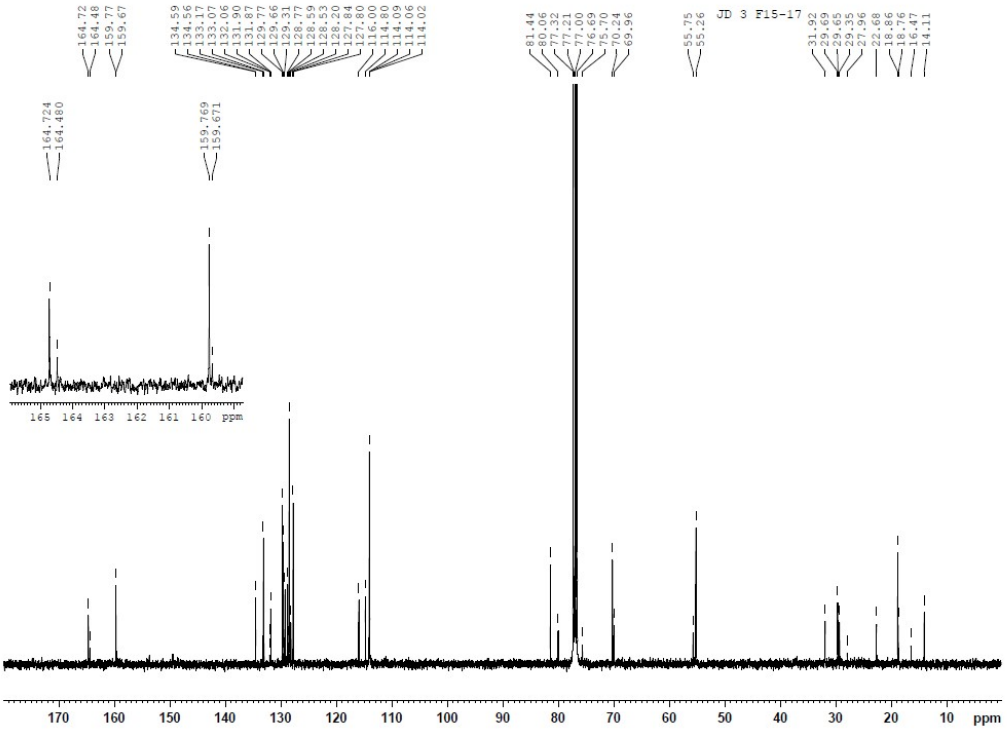

2. RMSD Analysis

A graphical representation of the RMSD values is presented in Figure S1. Low RMSD values indicate that the protein-ligand systems are well equilibrated and that compounds **6** and **8** maintained the binding pose anticipated in the inverted virtual screening stage. Compounds **6** and **8**, when bound to OBP, show a low RMSD contrary to AChE. This target displays higher values, which may suggest that there is an induced-fit adjustment to the AChE-binding pocket during the MD simulation. When looking at the RMSD of the ligands, compound **6** is the molecule that possesses lower RMSD values. This is mainly due to its own chemical structure, which is less flexible.

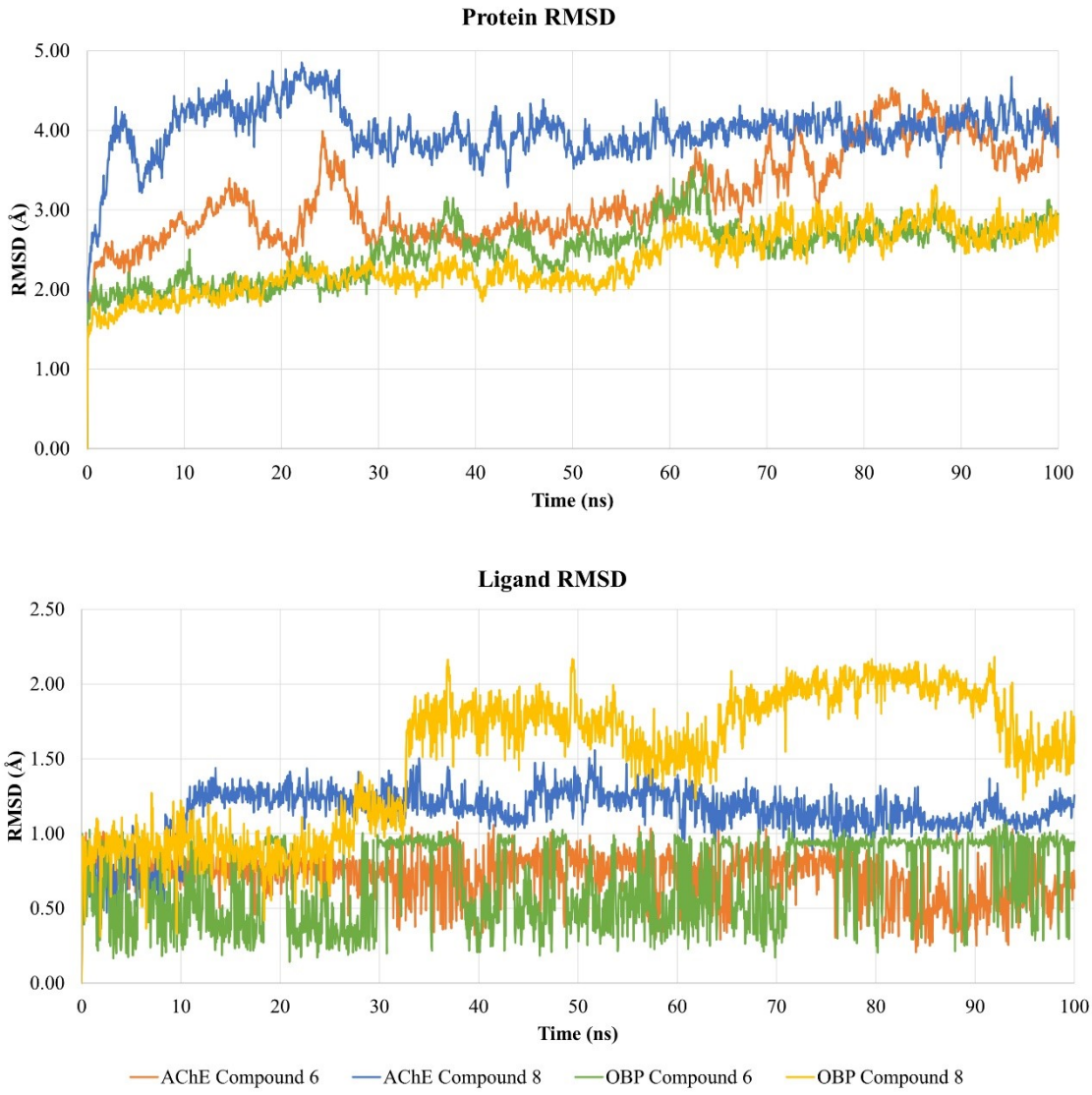

Figure S1. Protein and ligand RMSD (Å) of the AChE and OBP – ligand complexes.

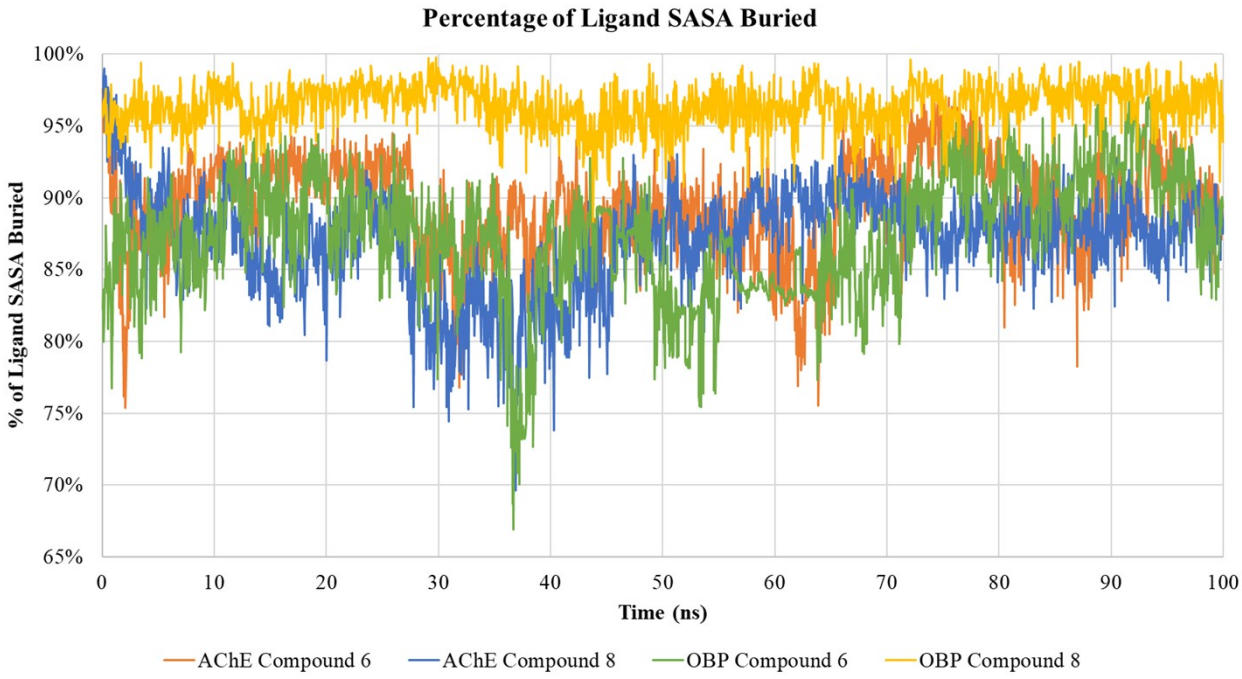

Figure S2. Variation of the percentage of potential ligand SASA buried by protein (%) when in complex with AChE and OBP.

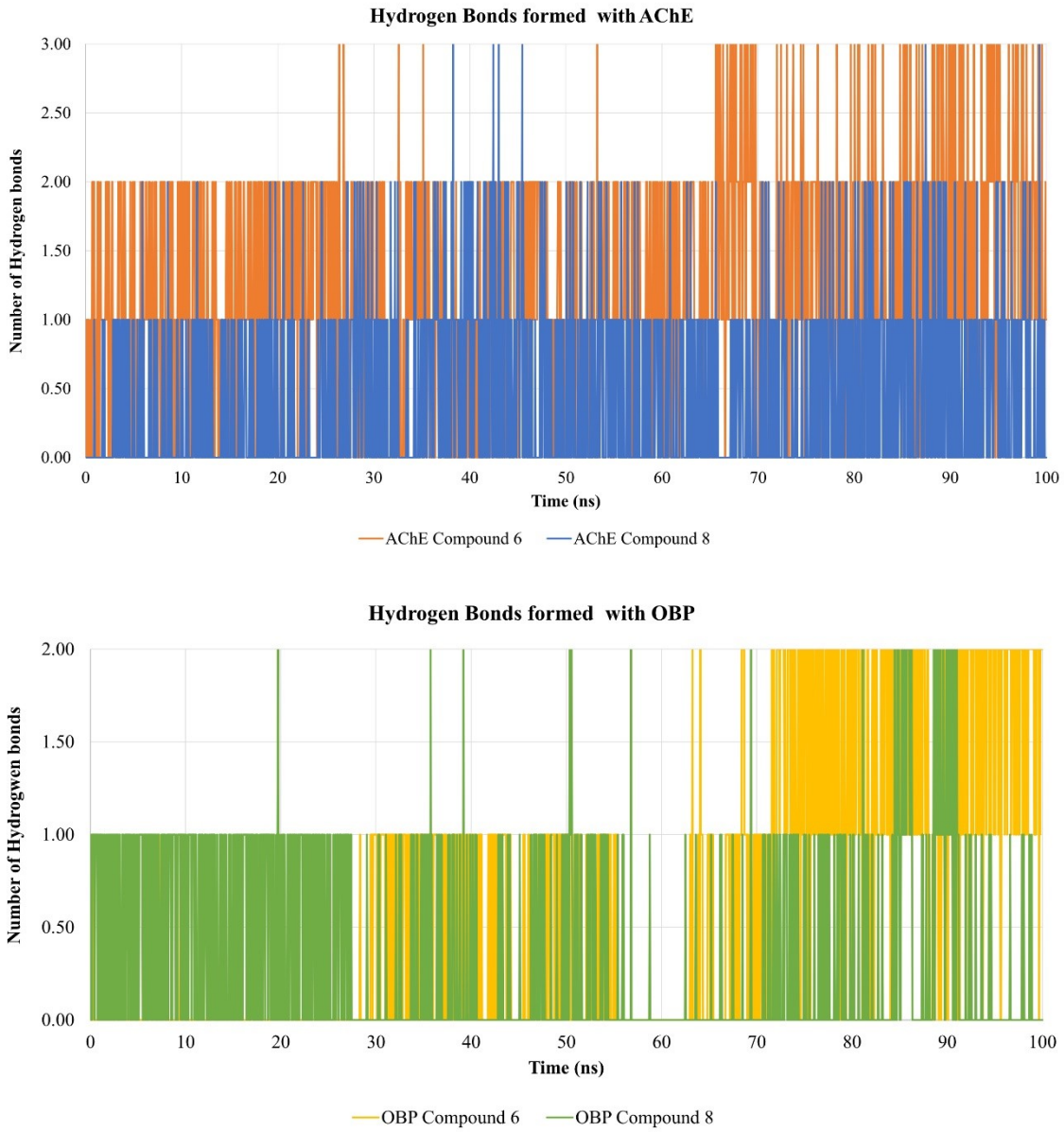

Figure S3. Hydrogen bonds formed throughout the simulation between AChE-compound **6**; compound **8** and OBP-compound **6**; compound **8**.

3. Creation of a homology model for 1QON

The SWISS-MODEL homology model created for the AChE molecular structure is shown in Figure S4. There are two metrics used to evaluate the quality of the model: GMQE and QMEAN. GMQE - Global Model Quality Estimation, which is expressed between 0 and 1 with a higher number meaning higher reliability. QMEAN - provides an estimate of the "degree of nativeness" of the structural features observed in the model. A value of QMEAN around zero indicate a good agreement between the model and experimental structure.

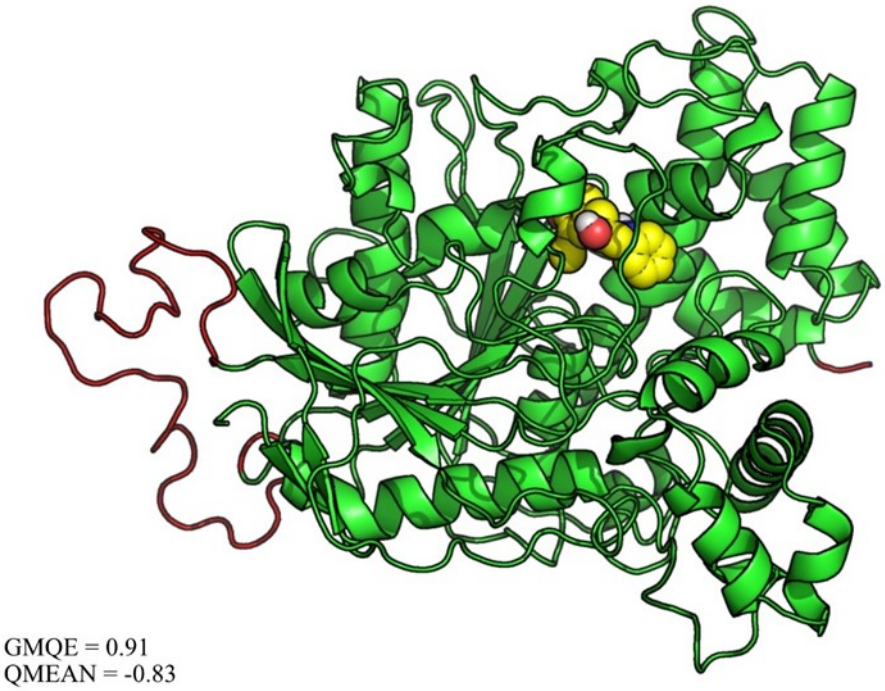

Figure S4. Homology model created for 1QON. Presented in green is the original structure. The only area that was built was the loop represented in red. An example of one of the ligands studied represented in yellow to illustrate that the area that was modelled is far from the active site.

Table S1. Average scores of compounds 6 and 8 against all the protein targets evaluated with the five different scoring functions. Overall ranking of the most likely protein targets for interaction.

Target	PDB	PLP	ASP	ChemScore	GoldScore	Vina	Overall ranking
Ecdysone receptor	**1R20**	53.60	24.36	27.34	42.29	-7.65	7
	1R1K	61.76	23.85	29.22	48.89	-8.30	
Chitinase	**3WL1**	67.02	34.59	28.88	47.86	-7.90	3
	3WQV	65.04	41.06	30.99	56.28	-7.80	
beta-*N*-acetyl-D-hexosaminidase OfHex1	**3OZP**	60.18	45.46	29.46	57.33	-7.30	4
	3NSN	65.70	38.69	28.23	54.04	-6.60	
N-Acetylglucosamine-1-phosphate uridyltransferase (GlmU)	**2V0K**	50.25	16.83	22.49	40.16	-7.10	12
	2VD4	43.77	18.73	20.24	38.70	-6.10	
Acetylcholinesterase	**1QON**	80.74	42.82	34.98	53.35	-9.80	2
	4EY6	63.53	32.14	31.85	52.20	-8.70	
	1DX4	68.13	33.73	29.94	48.72	-8.20	
Prophenoloxidase (PPO)	**3HHS**	45.59	16.01	19.11	46.26	-5.40	13
p-Hydroxyphenylpyruvate dioxygenase	**6ISD**	57.29	25.10	24.51	24.87	-7.20	9
Voltage-gated sodium channel	**6A95**	53.48	18.32	22.42	46.25	-6.60	11
Octopamine receptor	**4N7C**	45.21	33.21	37.59	41.31	-5.65	8
Sterol carrier protein-2 (HaSCP-2)	**4UEI**	56.94	31.26	32.57	48.87	-8.10	6
Peptide deformylase	**5CY8**	55.95	26.70	24.46	52.73	-5.30	10
α-Esterase-7	**5TYJ**	56.04	33.93	30.58	52.01	-7.10	5
	5TYP	56.29	35.23	32.03	54.43	-7.50	
Odorant binding protein	**5V13**	70.27	34.43	34.79	52.32	-8.50	1
	3K1E	73.06	36.41	34.38	55.92	-8.80	
	2GTE	63.90	34.64	35.77	56.02	-8.35	
	3N7H	65.42	34.01	30.95	57.93	-7.25	

Table S2. Docking scores for Human and Insect AChE when in complex with compounds **6** and **8**.

	Compound	PLP	ASP	ChemScore	GoldScore	Vina
Human AChE	**8**	69.42	41.22	35.15	63.06	-7.9
Insect AChE	**8**	92.19	60.29	42.82	70.73	-9.7
Human AChE	**6**	65.43	33.64	33.54	50.44	-8.6
Insect AChE	**6**	71.4	42.82	34.95	53.35	-9.8

Table S3. Targets selected for the inverted virtual screening assay

Target	Organism	PDB target	Resolution (Å)	Description	Ref
Ecdysone receptor	*Heliothis virescens*	1R20	3.00	VS based on 1R20 bound to an agonist as a model for the development of a receptor-based pharmacophore model.	1
		1R1K	2.90	VS of 2 million compounds against 1R1K, an ecdysone receptor structure bound to its known ligand ponasterone A.	2
Chitinase	*Ostrinia furnacalis*	3WL1	1.77	Pharmacophore-based screening using two crystal structures of chitinases: 3WL1 bound to its reaction product and 3WQV bound to an inhibitor.	3
		3WQV	2.04		
beta-*N*-acetyl-D-hexosaminidase OfHex1		3NSN	2.10	VS of the ZINC database to identify OfHex1 inhibitors using 3NSN crystal structure bound to a known inhibitor.	4
		3OZP	2.00	VS of the ZINC data-base targeting 3OZP, a crystal structure of OfHex1 bound to an inhibitor.	5
N-Acetylglucosamine-1-phosphate uridyltransferase (GlmU)	*Xanthomonas oryzae*	2V0K	2.30	Homology model built for docking using 2V0K and 2VD4 as templates. 2V0K crystal structure is bound to its known ligand and 2VD4 is bound to a possible inhibitor.	6
		2VD4	1.90		
Acetylcholinesterase	*Aedes aegypti*	1QON	2.72	Search for new molecules with insecticidal activity against *Ae. Aegypti* using acetylcholinesterase crystal structures 1QON and 4EY6 as targets, both bound to possible inhibitors.	7
		4EY6	2.40		
	Drosophila melanogaster	1DX4	2.70	Homology 3D model built for VS using 1DX4 as template. 1DX4 crystal structure is bound to a potent inhibitor.	8
Prophenoloxidase (PPO)	*Manduca sexta*	3HSS	1.97	Crystal structure of a prophenoloxidase from *Manduca sexta.*	9
p-Hydroxyphenyl-pyruvate dioxygenase	*Arabidopsis thaliana*	6ISD	2.40	Development of a receptor-ligand pharmacophore model based on the crystal structure 6ISD bound to a commonly used pesticide. The best model created was then used for VS studies.	10
Voltage-gated sodium channel	*Periplaneta americana*	6A95	2.60	Crystallographic structure of a Voltage-gated sodium channel NavPaS bound to a pore blocker, tetrodotoxin (TTX)	11
Octopamine receptor	*Blattella germanica*	4N7C	1.75	Crystal structure of Bla g 4, an octopamine receptor, bound to tyramine.	12
Sterol carrier protein-2 (HaSCP-2)	*Helicoverpa armigera*	4UEI	Solution NMR	Structure-based VS of a database of commercially available compounds to find potential inhibitors of HaSCP-2. The residues Phe53, Thr128, and Gln131 were selected for the binding cavity.	13
Peptide deformylase	*Xanthomonas oryzae*	5CY8	2.38	Docking and VS of a library of 318 phytochemicals. 5CY8 crystal structure is bound to a possible inhibitor.	14
Alpha-Esterase-7 (αE7)	*Lucilia cuprina*	5TYJ	1.75	Computational design of potent and selective covalent inhibitors of αE7. 5TYJ and 5TYP crystal structures are bound to inhibitors: (3-bromo-5-phenoxylphenyl)boronic acid and (3-bromo-4-methylphenyl)boronic acid, respectively.	15
		5TYP	1.88		
Odorant Binding Protein	*Aedes aegypti*	5V13	1.84	Search for new molecules with insecticidal activity against *Ae. Aegypti* using a crystal structure of a mosquito juvenile hormone-binding protein, 5V13 bound to its natural hormone.	7
	Drosophila melanogaster	2GTE	1.40	2GTE crystal structure is bound to its natural ligand.	16
	Anopheles gambiae	3N7H	1.60	QSAR and docking studies for the rational design of mosquito repellents using the crystal structure 3K1E bound to a polyethylene glycol molecule. 3N7H crystal structure is bound to a commonly used repellent.	17
	Aedes aegypti	3K1E	1.85		17

References

1. X. Hu, B. Yin, K. Cappelle, L. Swevers, G. Smagghe, X. Yang and L. Zhang, *J. Mol. Graph Model.*, 2018, **81**, 77-85.

2. T. Harada, Y. Nakagawa, T. Ogura, Y. Yamada, T. Ohe and H. Miyagawa, *J. Chem. Inf. Model.*, 2011, **51**(2), 296-305.

3. Y. Dong, X. Jiang, T. Liu, Y. Ling, Q. Yang, L. Zhang and X. He, *J. Agric. Food Chem.*, 2018, **66**, 3351-3357.

4. J. Liu, M. Liu, Y. Yao, J. Wang, Y. Li, G. Li and Y. Wang, *Int. J. Mol. Sci.*, 2012, **13**, 4545-4563.

5. L. Dong, S. Shen, Y. Xu, et al., *J. Biomol. Struct. Dyn.*, 2021, **39**, 1735-1743.

6. J. Min, D. Lin, Q. Zhang, J. Zhang and Z. Yu, *Eur. J. Med. Chem.*, 2012, **53**, 150-158.

7. R. Ramos, J. Costa, R. Silva, G. Costa, A. Rodrigues, E. Rebelo, R. Souto, C. Taft, C. Silva, J. Rosa, C. Santos and W. Macêdo, *Pharmaceuticals*, 2019, **12**, 20.

8. C. Riva, P. Suzanne, G. Charpentier, F. Dulin, M. Halm-Lemeille and J. Sopkova-de Oliveira Santos, *Pestic. Biochem. Physiol.*, 2019, **160**, 11-19.

9. Y. Li, Y. Wang, H. Jiang and J. Deng, *Proc. Natl. Acad. Sci.*, 2009, **106**, 17002-17006.

10. Y. Fu, Y. Liu, T. Kang, Y. Sun, J. Li and F. Ye, *J. Taiwan Inst. Chem. Eng.*, 2019, **103**, 33-43.

11. H. Shen, Z. Li, Y. Jiang, X. Pan, J. Wu, B. Cristofori-Armstrong, J. Smith, Y. Chin, J. Lei, Q. Zhou, G. King and N. Yan, *Science*, 2018, **362**(6412), 1-8.

12. L. Offermann, S. Chan, T. Osinski, Y. Tan, F. Chew, J. Sivaraman, Y. Mok, W. Minor and M. Chruszcz, *Mol. Immunol.*, 2014, **60**, 86-94.

13. J. Cai, X. Du, C. Wang, J. Lin and X. Du, *J. Econ. Entomol.*, 2017, **110**, 1779-1784.

14. T. Joshi, T. Joshi, P. Sharma, S. Chandra and V. Pande, *J. Biomol. Struct. Dyn*., 2021, **39**, 823-840.

15. G. Correy, D. Zaidman, A. Harmelin, S. Carvalho, P. Mabbitt, V. Calaora, P. James, A. Kotze, C. Jackson and N. London, *Proc. Natl. Acad. Sci*., 2019, **116**, 21012-21021.

16. J. Laughlin, T. Ha, D. Jones and D. Smith, *Cell*, 2008, **13**, 1255-1265.

17. P. Oliferenko, A. Oliferenko, G. Poda, D. Osolodkin, G. Pillai, U. Bernier, M. Tsikolia, N. Agramonte, G. Clark, K. Linthicum and A. Katritzky, *PLoS One,* 2013, **8**, e64547.